Effect of chloride concentration on the repassivation behavior of structural Al alloys

E. Melilli, M. Trueba, S.P. Trasatti

The present work reports on the effect of chloride concentration on the repassivation behavior of commercial aluminum alloys Al 5754-H111, Al 5083-H111, Al 2024-T3 and Al 7075-T6. Characteristic parameters of pitting and repassivation processes were determined from single cycle anodic polarization curves recorded in different NaCl solutions. Empirical relationships of the characteristic parameters as a function of log [Cl⁻] were derived from repeated experiments. Data analysis was complemented by corrosion morphology examination. Overall results show that valuable information on the corrosion resistance of different Al alloys can be obtained from the polarization response during the reverse scan. In the presence of localized attack other than pitting, the passivation of active surfaces follows a more complex mechanism.

Keywords: Al alloys - Corrosion - Electrochemistry

INTRODUCTION

Limited understanding of the relationships between microstructure and material performance represents an important technical barrier to the development of the aluminum technology. The mechanism of localized corrosion initiation and of the metastable-to-stable pit growth processes have been intensively investigated, mostly under the influence of Cl^- [1,2], and many models based on different approaches have been proposed [1-6]. Prediction of localized corrosion occurrence has been principally discussed on the basis of empirical approaches, mainly by considering the critical pitting potential (E_{pit}) [7,8]. Related studies on localized corrosion other than pitting [9-11] and on the repassivation mechanism of Al alloys [12-17] are scarce.
From our systematic studies of different commercial Al alloys in NaCl solution by single cycle anodic polarization, herein refereed as pitting scan (PS), the polarization behavior during the reverse scan provides valuable information about the repassivation processes [18-20]. Figure 1 shows the characteristic parameters that can be obtained from the PS curve. In particular, an inflection (at E_{ptp} and i_{ptp}) during reverse polarization scan into the active region indirectly manifests a transition to more occluded corrosion front due to favored micro-environment conditions for reactivation of localized attack rather than repassivation of all corroded surfaces. This characteristic has been overlooked in most studies on pitting of aluminium alloys, mostly because only the forward scan of the polarization is commonly recorded. However, the transition is very sensitive to the experimental conditions and depends on Al alloy nature [18-20 and ref. therein]. The investigation of the effect of chloride concentration [Cl^-], solution pH and dissolved oxygen on the repassivation behavior of Al 6082-T6 showed that $E_{ptp} \cong E_{pit}$ and $i_{ptp} > i_{pit}$ in diluted acid solutions [29]. Accordingly, E_{ptp} can be considered as the characteristic potential of the acidified pit-like solution in contact with a freshly created new surface. Thus, differently from Epit (for initially passive surface), E_{ptp} corresponds to the thermodynamic driving force for Al dissolution on freshly created surfaces. Similarly, i_{ptp} can be related to the rate at which hydrolysis equilibrium is reached for occluded chemistry conditions onset. From relationships of log i_{ptp} as a function of log [Cl^-], reaction orders between 1 and 2 indicated localized attack reactivation associated to formation of basic chloride aluminium salts like $Al(OH)Cl_2$ and $Al(OH)_2Cl$ species that weaken passive film formation and favor further pit nucleation. In addition, anodic dissolution controlled by proton reduction after the transition onset was suggested from the analysis of the steepness (stp) below E_{ptp} (Fig. 1).
In this work, the effect of [Cl^-] on the repassivation behavior of Al alloys such as Al 5754-H111, 5083-H111, Al 2024-T3, and Al 7075-T6, is investigated. Empirical relationships are derived to understand the transition to more-occluded local damage of Al alloys with different microstructure and localized corrosion behavior.

E. Melilli, M. Trueba, S.P. Trasatti
Università degli Studi di Milano

Experimental part

The composition of the commercial wrought Al alloys (AVIOMETAL S.p.A.) is reported in Table 1. Prior to use, the metallic surfaces were wet ground with abrasive SiC paper up to 1200 grit, thereafter polished with a 3 µm cloth using ethanol and solvent-cleaned in an ultrasonic bath.
PS were recorded at room temperature using a single-compartment O-ring cell, a Pt spiral as counter electrode and a Haber-Luggin capillary reference probe with a sa-

Fig. 1 - Schematic representation of characteristic parameters of pitting and repassivation processes: E_{corr} – potential after 10 min of conditioning at open circuit; E_{pit} and i_{pit} – potential and current density of pitting onset; E_{ptp} and i_{ptp} – pit transition potential and the corresponding current density at the inflection in the reverse scan; E_{prot} – protection potential; i_{rev} – current density limit of the forward scan; steepness (stp) – potential decrease with current below the inflection. The curve corresponds to experimental PS (10mVmin^{-1}) of polished Al6082-T6 [19].

Fig. 1 - Tipica curva di polarizzazione che mostra i parametri caratteristici dei processi di vaiolatura e ripassivazione: E_{corr} - potenziale in condizioni di circuito aperto dopo 10 min di stabilizzazione; E_{pit} e i_{pit} – potenziale e densità di corrente all'insorgenza della corrosione per vaiolatura; E_{ptp} e i_{ptp} - potenziale di transizione e corrispondente densità di corrente; E_{prot} - potenziale di protezione; i_{rev} - limite di densità di corrente della scansione d'andata. La curva corrisponde al PS sperimentale (10 mVmin^{-1}) della lega Al 6082-T6 lucidata [19].

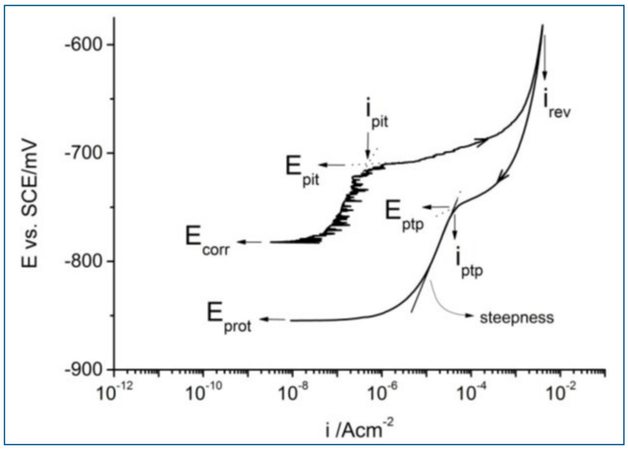

turated calomel electrode (SCE). The working electrode (active surface area of 1 cm^2) was positioned at the bottom of the cell (faced-up). Test solutions were prepared at different concentrations (0.1, 0.3 and 0.6 M) using NaCl (99.8%, Aldrich) and MilliQ water. The pH was adjusted to 5.6 (± 0.2) with HCl or NaOH addition. Anodic polarization was performed at 0.2 mVs^{-1} after 10-min of conditioning at open circuit in a given test solution. The current density limit of scan reversal (i_{rev}) was 2.5 mAcm^{-2}. Data were collected with a computer-driven PAR 273A potentiostat. At least three replicate experiments were performed for each testing condition. Graphical and quantitative analyses of the experimental data were carried out using OriginPro 9.0 program (OriginLab, Northampton, MA), as reported elsewhere [19].

Al alloys	Si	Fe	Cu	Mn	Mg	Zn	Ti	Cr
5754-H111	0.08	0.26	0.03	0.18	2.73	0.01	<0.01	0.05
5083-H111	0.17	0.32	0.04	0.62	4.32	0.03	0.02	0.07
2024-T3	0.15	0.25	4.67	0.63	1.34	0.02	0.06	0.01
7075-T6	0.04	0.13	1.60	0.02	2.52	5.90	<0.01	0.19

Table 1. Chemical composition (wt %) of commercial Al alloys

Tabella 1: Composizione chimica (% in peso) delle leghe commerciali di Al

The morphology of corroded specimens was examined using a LEO 1430 scanning electron microscope (SEM) equipped with an EDX spectrometer at a chamber pressure of 8 x 10^{-6} torr and 20 keV accelerating voltage. Cross-section specimens were embedded in a cold-working resin and polished up to 1 μm with diamond paste using ethanol.

RESULTS AND DISCUSSION

The PS of Al alloys resembled closely that shown in Fig. 1. Regardless Al alloy nature, the forward curves shifted to less negative potentials by increasing [Cl$^-$]. Similarly, the inflection shifted to smaller E_{ptp} and i_{ptp} values. Differences in the forward curves were manifested by the absence of an initial passive region for all substrates but Al 5083. This can be associated to more favored deposition of $SiO_2 \cdot nH_2O$ and/or $Mg(OH)_2$ due to electro(chemical) activity of Mg_2Si phase [18], as compared to Al 5754 with smaller content of Si and Mg (Table 1) and fine-grained microstructure. For Al 7075, two breakdown potentials were reproduced in this work [19], namely E_{pit1} (≅ E_{corr}) and E_{pit2} (at the peak in the current density for $E > E_{pit1}$). The latter characteristic indicates formation and dissolution of a silicon-rich corrosion film on the surface during the forward scan. Concerning the reverse scan, two inflections were distinguished only for Mg-rich alloys, being the second one very pronounced.

Corrosion morphology examination indicated differences in the corrosion front evolution with [Cl$^-$]. Mg-rich alloys show sharp dissolution fronts at pit bottoms in 0.1 M NaCl (Fig. 2a), indicating H-induced IG corrosion cracking catalyzed by the β phase (Al_3Mg_2) at grain boundaries [18]. By increasing further [Cl$^-$], cavities opening due to crystallographic pit growth was more important for Al 5754. In the case of Al 2024 (Fig. 2b), corrosion tunnels were observed for [Cl$^-$] ≤ 0.3 M, which suggests a decrease of the dissolution rate due to Cu accumulation at the surface [21]. Tunnel growth is not stable in 0.6 M NaCl, prevailing a transgranular fissuring. For Al 7075 (Fig. 2c), stress-induced fissures along grain borders due to IG penetration promote brittle failure.

Figure 3(a-c) shows the empirical relationships between the average electrochemical parameters and log [Cl$^-$]. Points missing in Fig. 3 correspond to conditions with indistinguishable inflection in the reverse curve. For series 5xxx alloys, E_{ptp1} (first transition) tends to values close to E_{pit} at [Cl$^-$] ≥ 0.3 M, whereas E_{ptp2} is shifted below the corresponding E_{pit} by 30-40 mV (Fig. 3a). It must be stressed out that only one transition (with E_{ptp} ≅ E_{ptp1}) was obtained with non-polished surfaces in 0.6 M NaCl (i_{rev} = 5 mAcm^{-2})

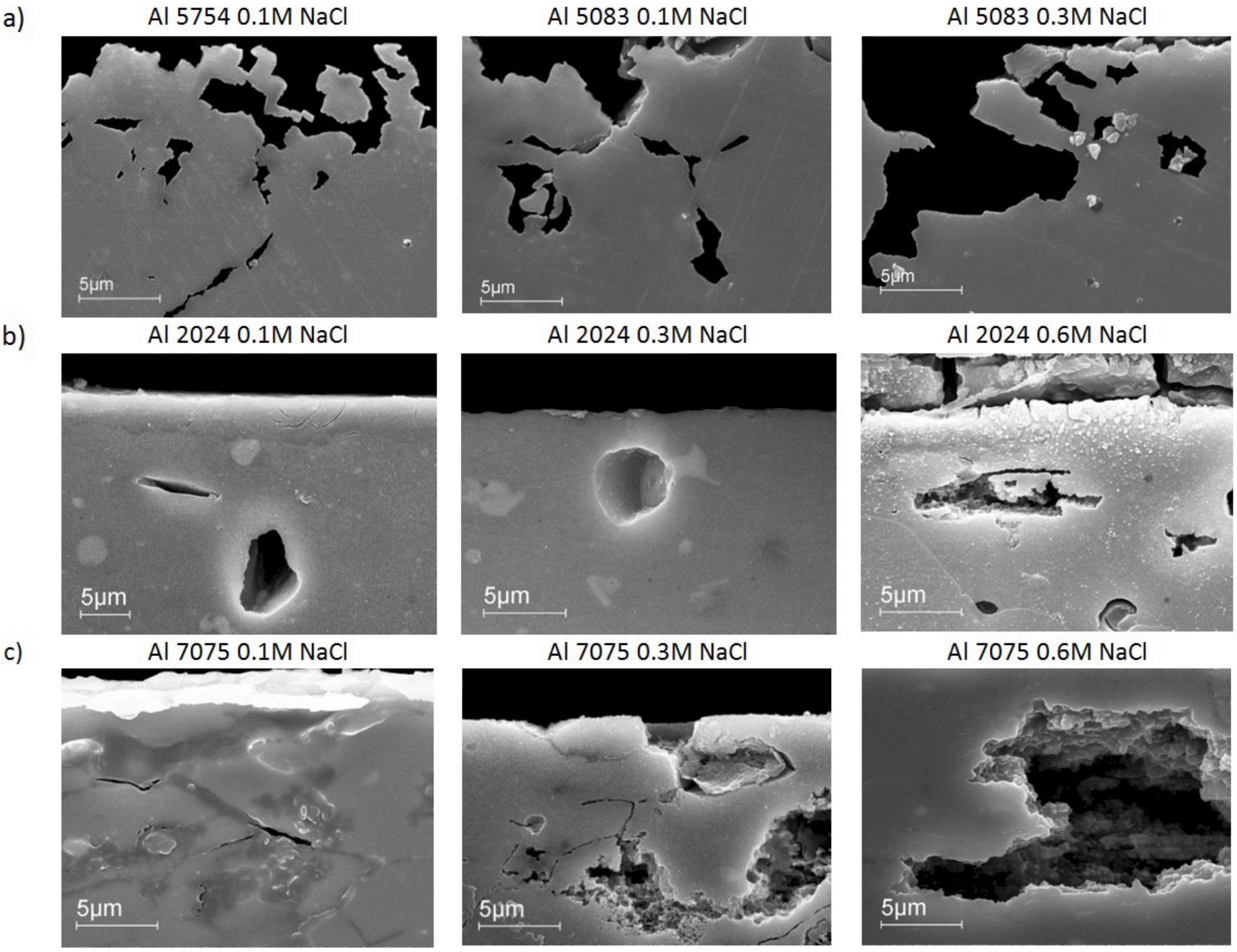

Fig. 2 - SEM images of cross-sectioned specimens after PS (0.2 mVs^{-1}, i_{rev} = 2.5 mAcm^{-2}) of Al alloys in different NaCl solutions (pH 5.6): (a) Mg-rich Al 5754 and Al 5083; (b) Al 2024; (c) Al 7075.

Fig. 2 - Immagini delle sezioni SEM dopo PS (0.2 mVs^{-1}, i_{rev} = 2.5 mAcm^{-2}) delle leghe di Al in differenti soluzioni di NaCl (pH 5.6): (a) Al 5754 e Al 5083; (b) Al 2024; (c) Al 7075.

[18]. In addition, E_{pit}, E_{ptp1} and E_{ptp2} decrease linearly with log [Cl^-]. The absolute slope values are similar to those obtained for Al 6082-T6 and pure Al in naturally aerated solutions (60 – 120 mVdec^{-1}) [20 and ref. therein]. The same result is obtained for E_{pit} and $E_{pit1,2}$ in the case of Al 2024 and Al 7075, with $E_{ptp} \cong E_{pit}$ (or E_{pit2} for Al 7075) as [Cl^-] increases (≥ 0.3 M) (Fig. 3a). However, higher the absolute slope values are estimated from Eptp vs log [Cl^-] (≅ 200 – 300 mVdec^{-1}), which indicates more important changes in local surface and solution compositions. By comparing Eptp values with previous data in 0.6 M solutions (NaCl 98%) and pH 6.5 [18,19], major differences are indicated for Al 2024 with 30-mV less negative E_{ptp} in this work. This suggests that this alloy is more sensitive to the composition of the test solution (impurities and/or initial pH).

The relationships between log iptp and log [Cl^-] (Fig. 3b) give absolute slope values close to 1 for Mg-rich alloys, except for the first transition in the case of Al 5754. These values allow estimation of the order of reaction with respect to [Cl^-] (n) [1,20], thus provide indication of the nature of the species involved in the transition onset. Accordingly, possible species involved in the second transition are $Al(OH)Cl_2$ and $Al(OH)_2Cl$, whereas less stable complex ions such as $AlCl^{2+}$ and $Al(OH)Cl^+$ are more likely for the first transition of Al 5083. For Al 5754 (Fig. 3b), n ≅ 0 indicates that the rate of equilibrium hydrolysis onset at E_{ptp}1 does not depend on [Cl^-], suggesting participation of loosely held chemisorbed species. IG attack is much less favored than crystallographic dissolution for this alloy, presenting fine-grained microstructure and more discontinuous β phase precipitates along gain boundaries as compared to Al 5083 [18]. The effect of temperature on the transition onset is currently investigated for clarifying the different dependence of E_{ptp1} with [Cl^-]. For Al 2024 and Al 7075, higher iptp and fractional n values (between 0.4 and 0.7) (Fig. 3b), suggest a more complex reaction mechanism during repassivation.

The plots of the steepness below the inflection in the reverse curve (Fig. 1) as a function of log [Cl^-] are shown in Fig. 3c. In the case of Mg-rich alloys, the steepness after the second transition (stp_2) is higher than that below the first inflection (stp_1), according to more pronounced de-

3a)

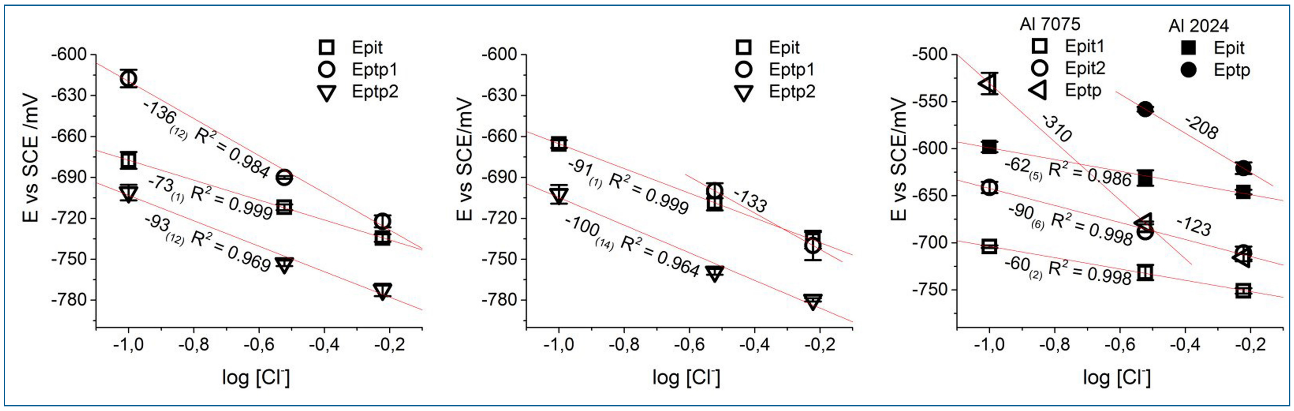

3b)

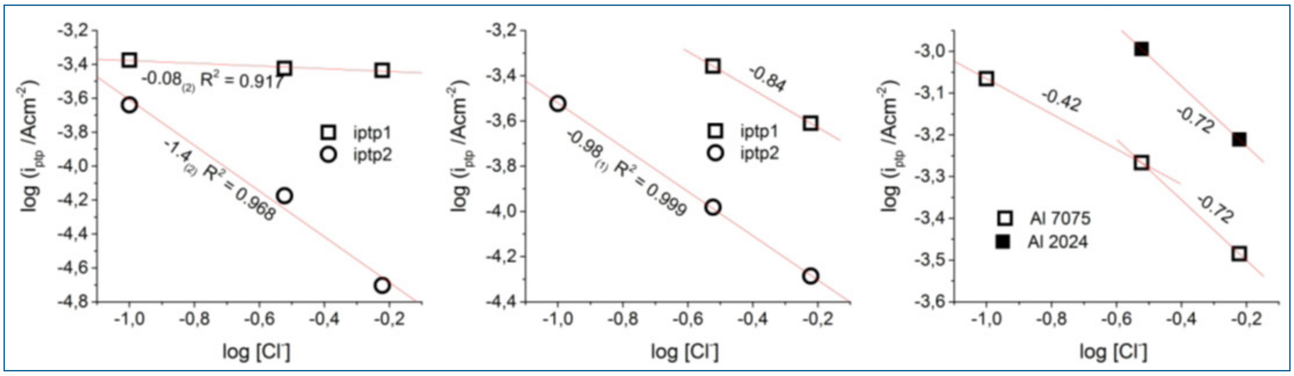

3c)

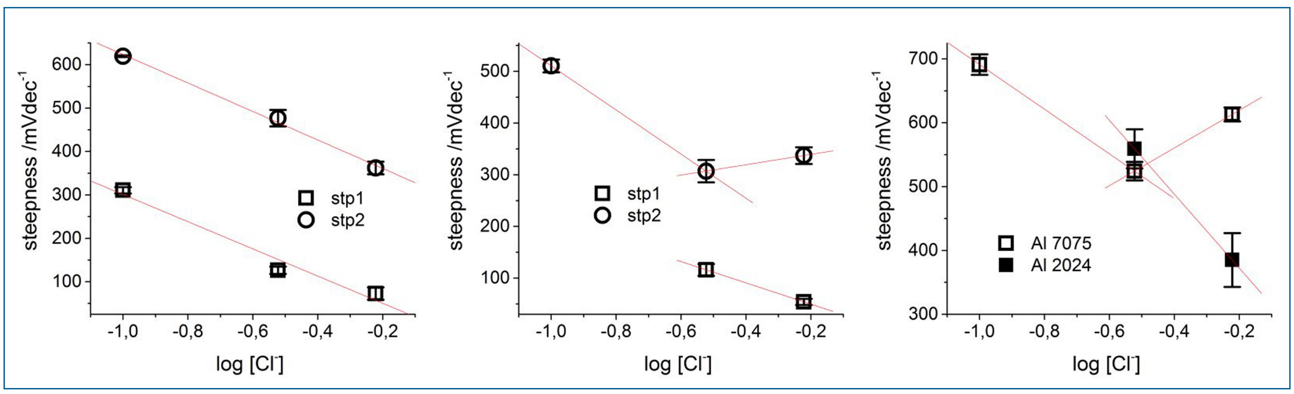

3d)

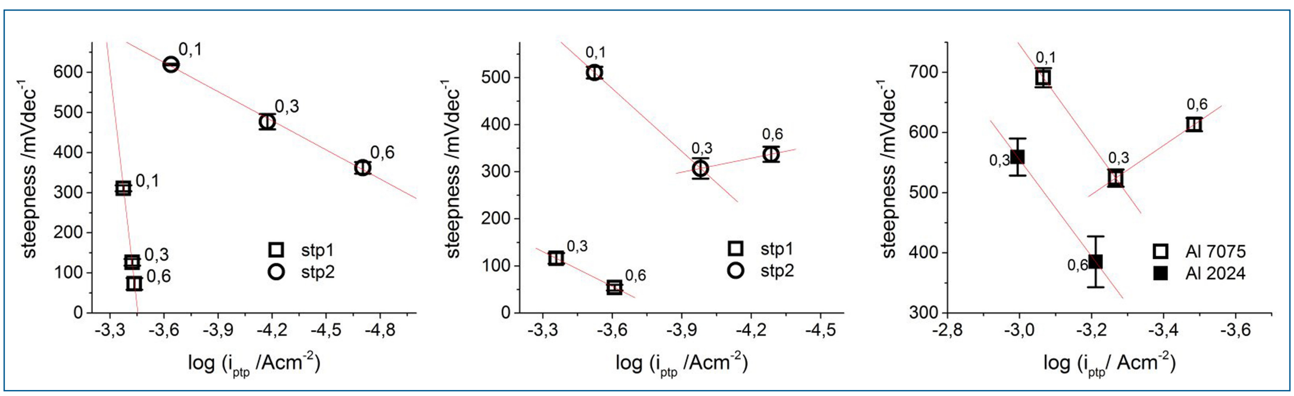

Fig. 3 - Empirical relationships between: (a-c) electrochemical parameters (Fig. 1) and log [Cl⁻]; (d) steepness vs log i_{ptp}. The values near the lines in (a,b) correspond to slopes values as obtained by linear fitting. Labels near the symbols in (d) indicate the corresponding [Cl⁻]. Error bars represent standard deviation.

Fig. 3 - Relazioni empiriche tra: (a-c) parametri elettrochimiche (Fig. 1) e log [Cl⁻]; (d) pendenza vs. log i_{ptp}. I numeri riportati accanto a ogni curva in (a,b) corrispondono ai valori della pendenze delle rette ottenute per regressione lineare. Nel grafico (d), è mostrato il valore di [Cl⁻]. La deviazione standard è riportata nella barra di errore.

crease of the potential below E_{ptp2}. For Al 5754, stp1 and stp2 decrease linearly with log $[Cl^-]$, which indicates that repassivation by dilution of occluded cavity solution is less limited as pitting corrosion is promoted, as obtained for Al 6082-T6 [20]. Conversely, stp2 increases for $[Cl^-] \geq 0.3$ M in the case of Al 5083. A similar difference in the trend of the steepness with $[Cl^-]$ (≥ 0.3 M) is obtained between Al 2024 and Al 7075 (Fig. 3c). From the plots of steepness vs. log iptp (Fig. 3d), the inflection shifts to smaller iptp values and the steepness decreases with $[Cl^-]$, except for Al 5083 (stp_2) and Al 7075. This correlates with less favored transition to more occluded corrosion front by promoting cavities opening towards the outer surface. The different behavior of Al 5083 and Al 7075 manifests a change in the repassivation mechanism as salt precipitation is promoted by increasing $[Cl^-]$. Based on corrosion morphology analysis (Fig. 2), this change could be associated to the onset of crevice corrosion for Al 5083 and to an embrittlement mechanism for Al 7075.

Additional experiments were carried out using smaller surface active area (0.1 cm^2) and higher scan rates (5 – 20 mVs^{-1}), also with specimens positioned on one side of the O-ring cell. The inflection in the reverse curve was more marked when deposition of corrosion products is assisted by gravity (faced-up specimens). In addition, only for Al 2024 the inflection was more pronounced by increasing the scan rate, in particular for $[Cl^-] = 0.6$ M. This correlates with tunnel growth destabilization by salt precipitation [21], as well as with time effects on conditions favoring corrosion tunnels [22]. The delay time associated to pit solution dilution is not enough for sustaining the local chemistry for tunnel growth when the scan rate is high.

CONCLUSIONS

The repassivation behavior of Al 5754, Al 5083, Al 2024 and Al 7075 was investigated as a function of chloride concentration by means of single cycle anodic polarization. The quantitative analysis of the polarization response during the potential scan into the active region allows discerning the propensity towards localized attack other than pitting of different Al alloys. In addition, the empirical relationships provide information about the repassivation mechanism by considering thermodynamic and kinetic aspects controlling the transition to more occluded local damage. In particular, the transition onset as related to formation of poorly protective corrosion films is confirmed. The approach used in this work reveals as a valuable electrochemical methodology for evaluating relationships between Al alloy composition/microstructure and corrosion resistance.

REFERENCES

[1] R.T. Foley, Corrosion 42 (1986) 277.
[2] Z. Szklarska-Smialowska Corros. Sci. 41 (1999) 1743.
[3] O. Guseva, P. Schmutz, T. Suter, O. von Trzebiatowski, Electrochim. Acta 54 (2009) 4514.
[4] E. McCafferty, J. Electrochem. Soc. 157 (2010) C382.
[5] L.C. Abodi, J.A. DeRose, S. Van Damme, A. Demeter, T. Suter, J. Deconinck, Electrochim. Acta 63 (2012) 169.
[6] O. Guseva, J.A. DeRose, P. Schmutz, Electrochim. Acta 88 (2013) 821.
[7] G. Engelhardt, D.D. Macdonald, Corros. Sci. 46 (2004) 2755.
[8] A. Anderko, N. Sridhar, D.S. Dunn, Corros. Sci. 46 (2004) 1583.
[9] W. Zhang, S. Ruan, D.A. Wolfe, G.S. Frankel, Corros. Sci. 45 (2003) 353.
[10] M.L.C. Lim, J.R. Scully, R.G. Kelly, Corrosion 69 (2013) 35.
[11] N. Murer, N.A. Missert, R.G. Buchheit, J. Electrochem. Soc. 159 (2013) C265.
[12] J.A.S. Green, R.M. Latanision, W.G. Montague, Corrosion 28 (1972) 466.
[13] S. Uruya, N. Soga, Corrosion 46 (1990) 989.
[14] B.J. Wiersma, Y. Tak, K.R. Hebert, J. Electrochem. Soc. 138 (1991) 371.
[15] G.T. Burstein, R.J. Cinderey, Corros. Sci. 33 (1992) 475.
[16] S.T. Pride, J.R. Scully, J.L. Hudson, J. Electrochem. Soc. 141 (1994) 3028.
[17] K. L. Moore, J. M. Sykes, P. S. Grant, Corros. Sci. 2008, 50, 3233.
[18] M. Trueba, S.P. Trastatti, Mater. Chem. Phys. 121 (2010) 523.
[19] I. Comotti, M. Trueba, S.P. Trasatti, Surf. & Interf. Anal 45 (2013) 1575.
[20] D. Cicolin, M. Trueba, S.P. Trasatti, Electrochim. Acta 124 (2013) 27.
[21] The theory of stress corrosion cracking in alloys, J.C. Scully Ed., Maney & Son Ltd., England, 1971
[22] R.C. Newman, Corros. Sci. 37 (1995) 527.

Effetto della concentrazione di cloruro sulla ripassivazione di leghe strutturali di alluminio

Parole chiave: Alluminio e leghe - Corrosione - Elettrochimica

Il presente lavoro riporta lo studio dell'effetto della concentrazione di cloruro nella ripassivazione di leghe di alluminio commerciali Al 5754-H111, Al 5083-H111, Al 2024-T3 e Al 7075-T6, mediante polarizzazione anodica a singolo ciclo. Sono state ottenute relazioni empiriche dei parametri caratteristici in funzione del log $[Cl^-]$. I risultati evidenziano che è possibile ottenere informazioni sulla resistenza alla corrosione di differenti leghe di Al dalle caratteristiche della curva di polarizzazione durante la scansione di ritorno. In presenza di attacco localizzato diverso da vaiolatura, la ripassivazione delle superfici segue un meccanismo più complesso.